Journal of Oceanology and Limnology
Vol. 37 No. 6, P. 1795-1804, 2019
https://doi.org/10.1007/s00343-019-8228-4

Effect of the drag coefficient on a typhoon wave model*

WANG Zhifeng, GONG Yijie, CUI Junnan, DONG Sheng, WU Kejian**

Ocean University of China, *Qingdao 266100*, *China*

Received Sep. 18, 2018; accepted in principle Jan. 15, 2019; accepted for publication Mar. 18, 2019

Abstract The effect of the drag coefficient on a typhoon wave model is investigated. Drag coefficients for Pingtan Island are derived from the progress of nine typhoons using COARE 3.0 software. The wind parameters are obtained using the Weather Research and Forecasting model. The simulation of wind agrees well with observations. Typhoon wave fields are then simulated using the third-generation wave model SWAN. The wave model includes exponential and linear growths of the wind input, which determine the wave-growth mode. A triple triangular mesh is adopted with spatial resolution as fine as 100 m nearshore. The SWAN model performs better when using the new drag coefficient rather than the original coefficient.

Keyword: drag coefficient; typhoon wind; typhoon wave; numerical simulation

1 INTRODUCTION

Wave models have largely improved in recent years owing to developments in parameterization and numerical analysis, and the description of observations becoming more consistent. Roland and Ardhuin (2014) summarized that incorporating coastal reflections, currents, and the types of bottom sediment is vital to improving wave modeling, which researchers are primarily interested in.

The National Centers for Environmental Prediction (NCEP, Chalikov and Babanin, 2012) proposed a new multi-grid global forecast operational system based on the third-generation model WAVEWATCH III. The system provides model guidance with appropriate spatial resolution for areas of interest to the National Weather Service (NWS) and NCEP. Wang and Jiang (2012) added a new term for the source of spectral dissipation to the WAVEWATCH III model. A new spectral dissipation source term is proposed, which comprises saturation based dissipation above two times of peak frequency and improved whitecapping dissipation at lower frequency spectrum. Siadatmousavi et al. (2012) found that it is important that the assumptions used to evaluate high cut-off frequencies of different frequency components interacting in spectral evolution are different in the third-generation wave models SWAN and WAVEWATCH III, and that WAM cycle 3 is more sensitive than other versions of the WAM model to the cut-off frequency and the index of the frequency tail expression in SWAN. Furthermore, on the basis of the Courant-Friedrichs-Lewy criterion, Dietrich et al. (2013) proposed limiters in SWAN for spectral propagation velocities. These limiters reduce local errors and prevent the excessive directional turning and frequency shifting of wave energy so as to improve accuracy; errors otherwise spread throughout the computational field. Rascle and Ardhuin (2013) presented a multiscale global wave hindcast for the period 1994 to 2012 based on improved source term parameterizations for wind and swell dissipation. The effects of precisely expressing the wind force acting on a wave and surge modeling were studied by Bricheno et al. (2013).

Improved wave-directional clustering has been observed when using meteorological forcing of higher resolution. Using a modified version of Janssen' method (Janssen, 1991), Kim et al. (2015) investigated the effect of using a dependent drag coefficient of a wind-speed-limited wave on the generation of a wave for the super typhoon Haiyan and applied to a step

* Supported by the National Key Research and Development Program of China (No. 2016YFC1402000) and the National Natural Science Foundation of China (Nos. 51509226, 51779236)
** Corresponding author: kejianwu@ouc.edu.cn

function index wave of growth for a certain coefficient of horizontal resistance. Results showed that the existing method for wind speeds of 25–30 m/s is applicable to the coupled wave and surge model under the condition of a super typhoon. Lee (2015) investigated the capability of the wave model WAVEWATCH III with wind input and dissipation terms to reproduce the severe ocean conditions of October 2006. Fan and Rogers (2016) calculated drag coefficients for hurricane Ivan, which struck in 2004, from wave spectra simulated using WAVEWATCH III and scanning radar altimeter data. Tsai et al. (2018) studied general characteristics of wind waves and drag coefficients using the data of near-shore buoy observations recorded in Taiwan Strait.

Threats to the economy and property posed by large disasters are becoming increasingly serious as the economy rapidly grows in coastal areas of China. It is therefore important to establish and improve numerical predictions for coastal marine areas. The present paper investigates the effect of the drag coefficient on a typhoon wave model. The remainder of the paper is organized as follows. Section 2 introduces the Weather Research and Forecasting (WRF) wind model and its setup. Section 3 describes the setup of the wave model and the simulation process. Section 4 presents results and a discussion. Finally, Section 5 provides a summary and conclusions.

2 WIND FORCE

2.1 Description of the wind model

The wind field plays a major role in wave simulation. A suitable wind simulation is also necessary in forecasting waves. The present paper chooses a mesoscale forecasting mode and assimilation system WRF (Skamarock et al., 2008) mode for simulation of the wind field. A numerical weather forecast, data assimilation, and atmosphere simulation are combined on an Arakawa C grid to advance the forecast and simulation of mesoscale weather. In addition, the simulation model includes both physical and dynamic processes of climate change and an atmosphere radiation mode, which is in view of a short-wave and long-wave radiation scheme, cloud and ground surface layer.

In the vertical direction, η is defined as

$$\eta=(p_{\mathrm{h}}-p_{\mathrm{ht}})/\mu, \quad (1)$$

where $\mu=p_{\mathrm{hs}}-p_{\mathrm{ht}}$ while p_{hs} and p_{ht} are pressures.

The Euler form of the equation is

$$\frac{\partial U}{\partial t}+(\nabla\times V_u)-\mu_{\mathrm{d}}\alpha\frac{\partial p}{\partial x}+(\alpha/\alpha_{\mathrm{d}})\frac{\partial}{\partial\eta}\left(\frac{\partial p\partial\Phi}{\partial\eta\,\partial x}\right)=F_u, \quad (2)$$

$$\frac{\partial V}{\partial t}+(\nabla\times V_v)-\mu_{\mathrm{d}}\alpha\frac{\partial p}{\partial y}+(\alpha/\alpha_{\mathrm{d}})\frac{\partial}{\partial\eta}\left(\frac{\partial p\partial\Phi}{\partial\eta\,\partial y}\right)=F_v, \quad (3)$$

$$\frac{\partial W}{\partial t}+(\nabla\times V_w)-\mathrm{g}\left[(\alpha/\alpha_{\mathrm{d}})\frac{\partial p}{\partial\eta}-\mu_{\mathrm{d}}\right]=F_w, \quad (4)$$

$$\frac{\partial\Theta}{\partial t}+(\nabla\times V\theta)=F_\theta, \quad (5)$$

$$\frac{\partial\mu}{\partial t}+(\nabla\times V)=0, \quad (6)$$

$$\frac{\partial\varphi}{\partial t}+\frac{1}{\mu}\left[(V\times\nabla\varphi)-\mathrm{g}W\right]=0, \quad (7)$$

$$\frac{\partial Q_{\mathrm{m}}}{\partial t}+(\nabla\times Vq_{\mathrm{m}})=F_{Q_{\mathrm{m}}}, \quad (8)$$

where u is the zonal wind vector, v is the meridional wind vector, μ is the friction coefficient, g is the gravity coefficient, Φ is the geopotential, F is the external force, w is the vertical wind vector, θ is the potential temperature, π is the total Exner function, and Q_{m} and q_{m} are specific humidities.

2.2 Setup and validation of the wind model

The WRF model is run each hour with 16 vertical layers and a horizontal spatial resolution of 0.1° by 0.1°. The Yonsei University (YSU) scheme is applied to the lateral boundary. The NCEP reanalysis product, with a spatial resolution of 0.25° by 0.25° reported every 6 hours, is used for the initial field. We use two nested grids for the WRF model. The smaller research area covers 17°N to 28°N and 117°E to 127°E for the accurate simulation of offshore weather while the larger research area covers 103°E to 137°E and 5°N to 45°N for the capture of ocean conditions along all of the western coast of the East China Sea.

The WRF model offers a number of physical options, such as a cumulus parameterization scheme, atmospheric-boundary-layer turbulence scheme, cloud microphysics scheme, sea/land surface scheme, and shortwave radiation scheme. Table 1 gives the setup of the WRF model.

The data of six observation buoys (i.e., B1, B2, B3, 0022, 0023, and QF206) are used to validate the wind field. Figure 1 shows the locations of the six buoys. The data were recorded from January 2012 to October 2012.

Three statistical metrics are used to validate the wind field, namely the mean error (ME), mean absolute error (MAE), and root-mean-square error (RMSE):

$$\mathrm{ME}=\frac{1}{N}\sum_{i=1}^{N}\left(X_{\mathrm{mod}}^{i}-X_{\mathrm{obs}}^{i}\right), \tag{9}$$

$$\mathrm{MAE}=\frac{1}{N}\sum_{i=1}^{N}\left|X_{\mathrm{mod}}^{i}-X_{\mathrm{obs}}^{i}\right|, \tag{10}$$

$$\mathrm{RMSE}=\sqrt{\frac{\sum_{i=1}^{N}(X_{\mathrm{mod}}^{i}-X_{\mathrm{obs}}^{i})^{2}}{N}}, \tag{11}$$

where X_{mod}^{i} denotes the grid points of the WRF simulation data while X_{obs}^{i} denotes the grid points of the observation data.

Figure 2 compares the simulation and observation

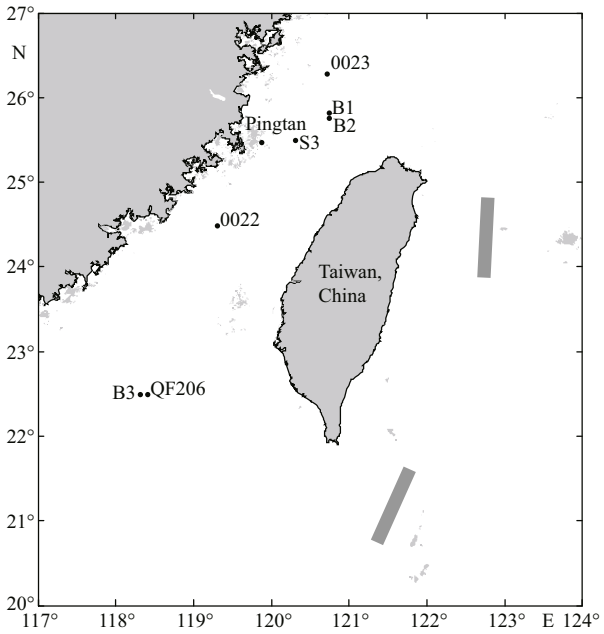

Fig.1 Distribution of observation buoys

Table 1 Setup of the WRF model

Physical progress	References
Boundary	YSU (Hong et al., 2006)
Cloud	Kain-Fritsch (Kain and Fritsch, 1990)
Rad	Long: RRTMG (Mlawer et al., 1997) Short: RRTMG (Dudhia, 1989)
Land	Noah (Decharme, 2007)

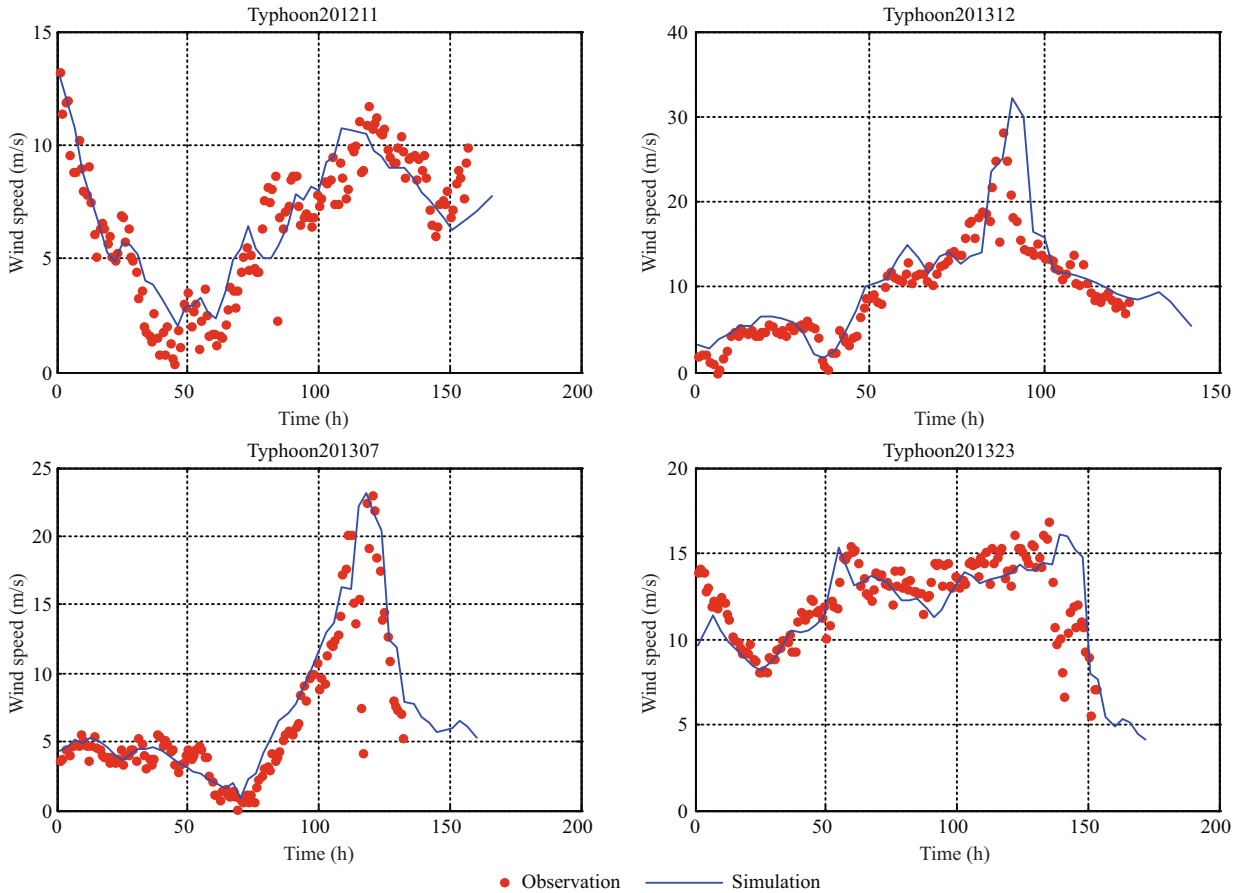

Fig.2 Comparison of wind-speed hindcast data and observation data

data. Relative to observation data, the ME ranges from 0.02 to 0.74, the MAE ranges from 1.05 to 2.11, and the RMSE ranges from 1.29 to 2.06. The simulation results therefore agree well with observation data in general.

3 WAVE SIMULATION

3.1 Description of the wave model

The SWAN spectral wave model is used in wave estimations. This numerical wave model allows realistic simulations of wave parameters for coastal areas, lakes, and estuaries according to the given wind, bottom friction, and current conditions. The model is a third-generation fully spectral model (Booij et al., 1999). Its theoretical basis was presented by Ris et al. (1999) and Zijlema and van der Westhuysen (2005).

The SWAN model uses action density $N(\sigma, \theta)$ instead of variance density $E(\sigma, \theta)$ to calculate the development of a sea state, because the current action density is more conserved than the variance density. The action density equals the variance density divided by the relative frequency:

$$N(\sigma, \theta)=E(\sigma, \theta)/\sigma, \quad (12)$$

where θ is the wave direction and σ is the relative frequency.

The spectral action balance equation states the evolution of the wave spectrum. This equation is written in Cartesian coordinates as

$$\frac{\partial N}{\partial t}+\frac{\partial}{\partial x}c_x N+\frac{\partial}{\partial y}c_y N+\frac{\partial}{\partial \sigma}c_\sigma N+\frac{\partial}{\partial \theta}c_\theta N=\frac{S}{\sigma}. \quad (13)$$

The first term on the left side of the equation is the local rate of change in the action density with time, the second term refers to propagation in the x direction with velocity c_x, the third term is the same as the second term but for the y direction, the fourth term is the shift in the relative frequency due to changes in current and water depth with propagation velocity c_σ, and the last term refers to the refraction of currents and water depth with propagation velocity c_θ, as derived from linear-wave theory. S is the source term, which represents the effects of dissipation, wind generation, and nonlinear wave-wave interactions. The main components of dissipation are bottom friction, white capping, and wave breaking due to a change in depth.

Three formulations are used to clarify the processes of wave generation with wind and white capping in the SWAN model.

1. The parameterization of Komen et al. (1984): this parameterization describes the transmission of energy from wind to waves attached by the pulse-based model of Hasselmann (1974), can be used for white capping, and can be used for a limited water depth as done by the WAMDI Group (1988).

2. The model of Janssen (1991): this model can be used for meteorological input attached by the same pulse-based model of Hasselmann (1974) and can be used for white capping.

3. The model of Yan (1987): this model can be used for meteorological input attached by the saturation-based model of Alves and Banner (2003) and can be used for white capping.

Wind can also state linear and index increase. The first formulation considers that Cavaleri and Malanotte Rizzoli (1981) used a filter to simulate the generation of waves at frequencies lower than Pierson-Moskowitz frequencies (Tolman, 1992). In terms of exponential growth, two statements are effective, the first provided by (Komen et al., 1984) and these condone provided by Janssen (1991).

There are two methods of describing nonlinear mutual wave-wave effects in deep water: XNL (i.e., the WRT method) and discrete interaction approximation. The discrete interaction approximation of Hasselmann et al. (1985) is usually used to estimate quadruplets in SWAN and thus improve the calculation efficiency. Rusu et al. (2008) found that discrete interaction approximation performed well for a Portuguese coastal area.

3.2 Model setup and simulation process

The wave model assumes the spherical coordinates of a nonstationary mode. The implementation of the model was made for 36 directions and 30 frequencies logarithmically spaced from 0.05 Hz to 1.0 Hz at intervals of $\Delta f/f$=0.1. It is assumed that there is no current. Calculations are made with a time step of 20 min in a nonstationary mode. The number of iterations is set from 1 (the default value) to 4, to increase the numerical accuracy when the model passes to another time step.

The model includes exponential and linear growths of wind input because, as described by Moeini et al. (2010), this allows more accurate forecasting the significant wave height. The model is based on the wind input parameterization developed by Komen et al. (1984) for an exponential increase in wind input. The wind drag parameterization derived above is similar to the parameterization of Zijlema et al.

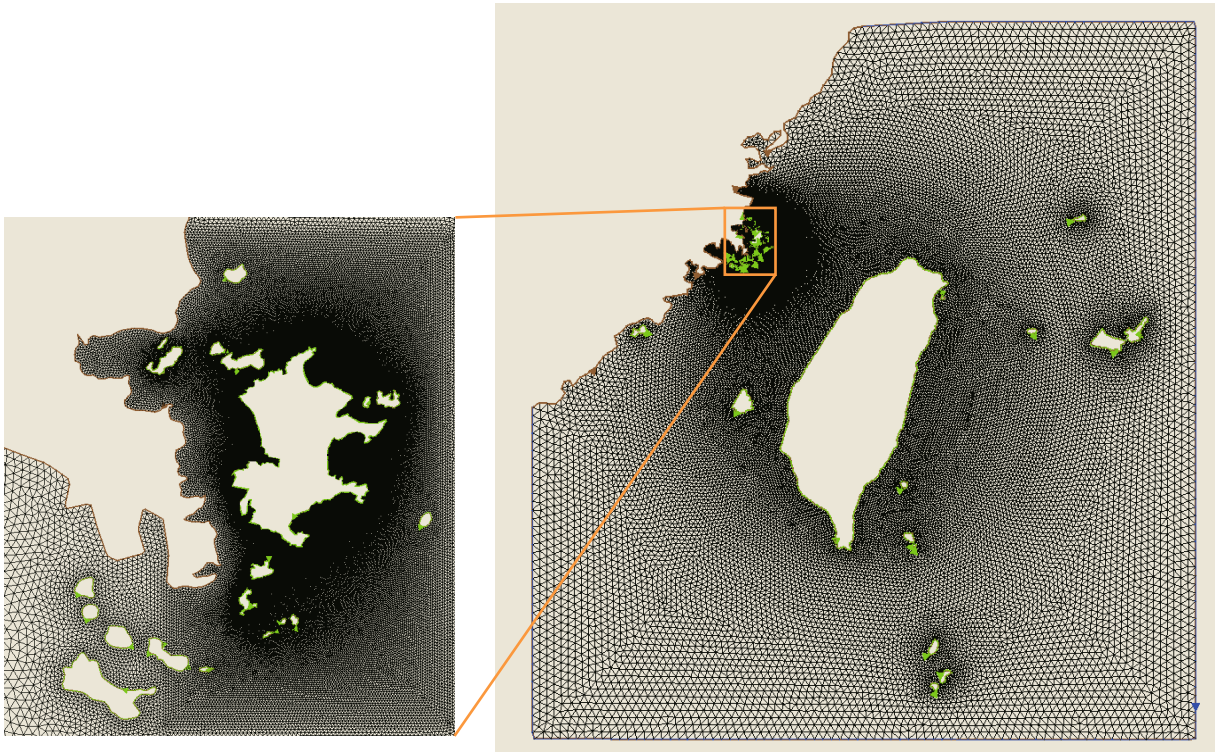

Fig.3 Triple triangular mesh of the wave forecast model

Table 2 Physical processes in the hindcast study

Physical processes	SWAN model
Linear wind input and growth	Cavaleri and Malanotte Rizzoli (1981)
Exponential wind input and growth	Komen et al. (1984)
Whitecapping dissipation	Komen et al. (1984)
Non-linear interaction (quad.)	Hasselmann et al. (1985).
Non-linear interaction (triad)	Eldeberky (1996)
Bottom friction dissipation	JONSWAP

(2012). The present simulation considers dissipation due to bottom friction, wave breaking, and white capping. The interactions of quadruplet and triad waves are respectively taken as nonlinear interactions for shallow and deep waters. Table 2 presents the physical processes in the hindcast study.

The reasonable setting of boundary conditions is an important consideration of the present paper. Waves within the computation area might be strongly affected by waves at the boundary. A triple triangular mesh with fine precision is adopted for the wave forecast model. The largest grid of the mesh covers 117°E–125°E and 19.5°N–28°N and has a resolution of 3′–6′. The second grid has a resolution of 0.24′–3′. The smallest grid covers the area 119.5°E–120°E and 25.15°N–25.8°N near Pingtan Island and has a resolution 100–400 m. The fine resolution of 100 m near Pingtan Island shows changes for the nearshore terrain. Grid maps are shown in Fig.3. The water depth on the large grid is taken from ETOPO1 data while that on the fine grid near Pingtan Island is observation data (Fig.4). The wide coverage of Taiwan Strait allows simulation of the regularity of wave transformation during a typhoon completely, while the fine coverage allows precise simulation of wave conditions near Pingtan Island.

4 RESULT AND DISCUSSION

4.1 Drag coefficient

Researchers have introduced many parameterization schemes for the sea surface roughness z_0 based on data recorded by buoys, towers, and ships. Charnock (1955) put forward a now well-known formula to estimate the sea surface roughness:

$$\frac{gz_0}{u_*^2}=\alpha\,, \tag{14}$$

where g is the acceleration due to gravity while α is a universal constant. Different values of α have been given by different researchers; e.g., α=0.012 given by Charnock (1955), α=0.013 by Smith and Banke (1975), and α=0.018 5 by Wu (1982).

The general bulk-flux algorithm COARE 3.0 (Fairall et al., 2003) offers three optional

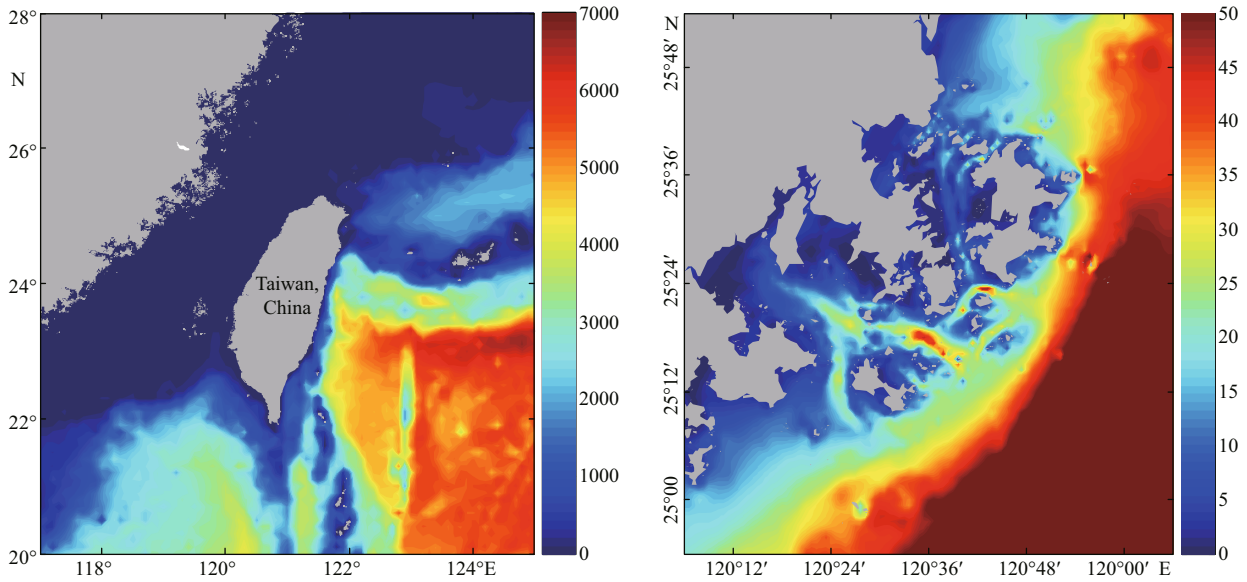

Fig.4 Depth setup for the SWAN model

parameterizations of the roughness, one of which considers the surface wind friction velocity. The velocity roughness length is specified as Charnock's (1955) expression plus a smooth flow limit, following Smith (1988):

$$z_0 = \alpha u_*^2 / \mathrm{g} + 0.11\nu / u_*, \quad (15)$$

where ν is the kinematic viscosity. The COARE flux data proposed the Charnock parameter value of Smith, α=0.011.

The second parameterization considers the wave height and steepness (Taylor and Yelland, 2001):

$$z_0 = 1200 H_s \left(H_s / L_p\right)^{4.5} + 0.11\nu / u_*. \quad (16)$$

The third parameterization considers the wavelength and the inverse of the wave age (Oost et al., 2002):

$$z_0 = 25 / \pi L_p \left(u_* / C_p\right)^{4.5} + 0.11\nu / u_*. \quad (17)$$

The vertical profile of the wind speed versus height is given as

$$u_{10} = \frac{u_*}{\kappa} \ln\left(\frac{10}{z_0}\right), \quad (18)$$

where the von Karman velocity κ is 0.40. The roughness length and neutral drag coefficient of 10 m are then related as (Vickers et al., 2013)

$$C_\mathrm{d} = \left[\frac{\kappa}{\ln\left(10 / z_0\right)}\right]^2. \quad (19)$$

The original drag coefficient used in the SWAN model was given by Wu (1982):

$$C_\mathrm{d}=0.8+0.065U_{10}. \quad (20)$$

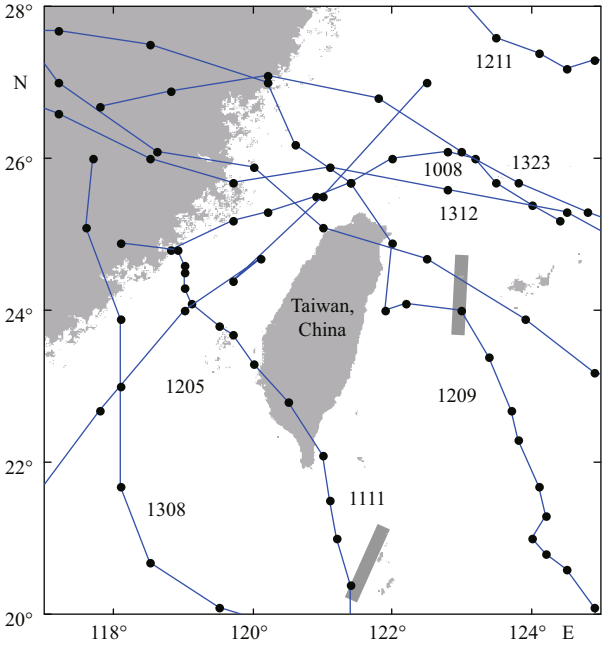

Fig.5 Tracks of nine typhoons affecting Pingtan Island

By reviewing many observations, Zijlema et al. (2012) proposed a new wind drag parameterization where by the wind drag decreases at high wind speed:

$$C_\mathrm{d}\times 10^3 = 0.55 + 2.97\tilde{U} - 1.49\tilde{U}^2, \quad (21)$$

where $\tilde{U}=U_{10}/U_{\mathrm{ref}}$, with the reference wind U_{ref}=31.5 m/s being the wind speed at which C_d is a maximum according to this equation.

To obtain a reasonable drag coefficient for Pingtan Island, we take nine typhoons (blue lines in Fig.5) and fit a second-order polynomial to observations. Fitted curves are shown in Fig.6. We adopt an extremely low wind speed (5 m/s). We have

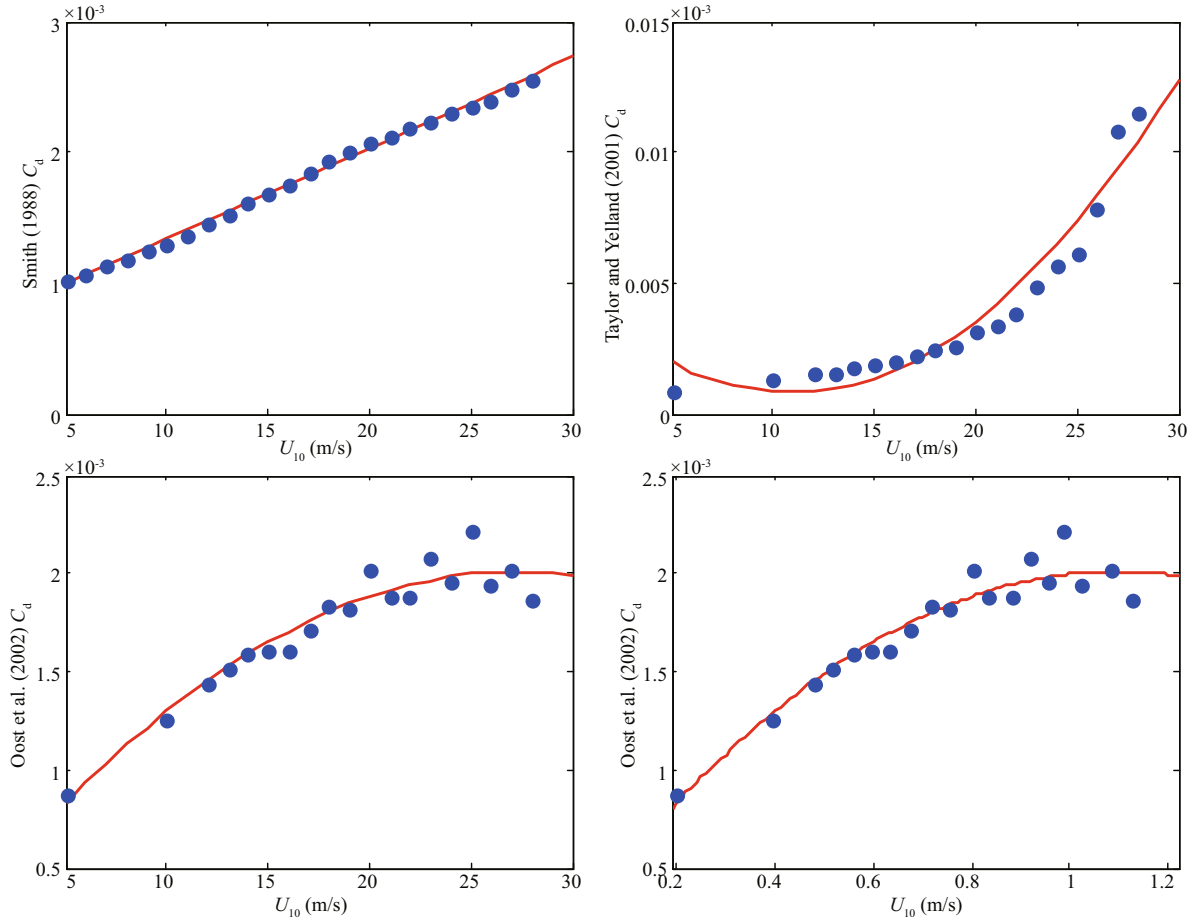

Fig.6 Fitted curves of the drag coefficient obtained by COARE 3.0

$$C_d \times 10^3 = A + BU_{10} + CU_{10}^2, \quad (22)$$

or

$$C_d \times 10^3 = A + B\tilde{U} + C\tilde{U}^2. \quad (23)$$

The parameters A, B, and C from COARE 3.0 are given in Table 3.

Table 3 Parameters *A*, *B*, and *C* from COARE 3.0

Formula	A	B	C	R^2
(Smith, 1998) with U_{10}	0.65	0.069	-	0.99
(Taylor and Yelland, 2001) with U_{10}	4.7	-0.72	0.033	0.94
(Oost et al., 2002) with U_{10}	0.25	0.13	-0.024	0.93
(Oost et al., 2002) with $\tilde{U}$	0.25	3.2	-1.5	0.93

- means no data.

4.2 Simulation results

Donelan et al. (2004), guided by the results of extreme wind experiments conducted in the laboratory, showed that the aerodynamic roughness approaches a limit in high winds. Takagaki et al. (2016) suggested that the peak enhancement factor of the wind-sea spectrum decreases with a decreasing inverse wave age and with an increasing wind speed. Zhao and Li (2018) found that in high winds, intense wave breaking results in the collapse of the relationship between the wave steepness and wave age, and the drag coefficient decreases with a decreasing wave age and levels off with an increasing wind speed. Following these previous studies, the values of Oost et al. (2002) are finally adopted:

$$C_d \times 10^3 = 0.25 + 3.2\tilde{U} - 1.5\tilde{U}^2. \quad (24)$$

The results of two buoy stations (0023 and S3) in Taiwan Strait are used in validation of the simulation. The locations of the wave buoys are shown in Fig.1. The progress of four typhoons (1211, 1307, 1312, and 1323 shown in Fig.4) is selected to validate the simulation results of SWAN. The validation results are presented in Fig.7. We compare the hindcast data with observation data. There is good agreement between the simulation and observation data.

Table 4 gives the average relative error (ARE) and MAE during the four typhoons. The ARE is calculated as

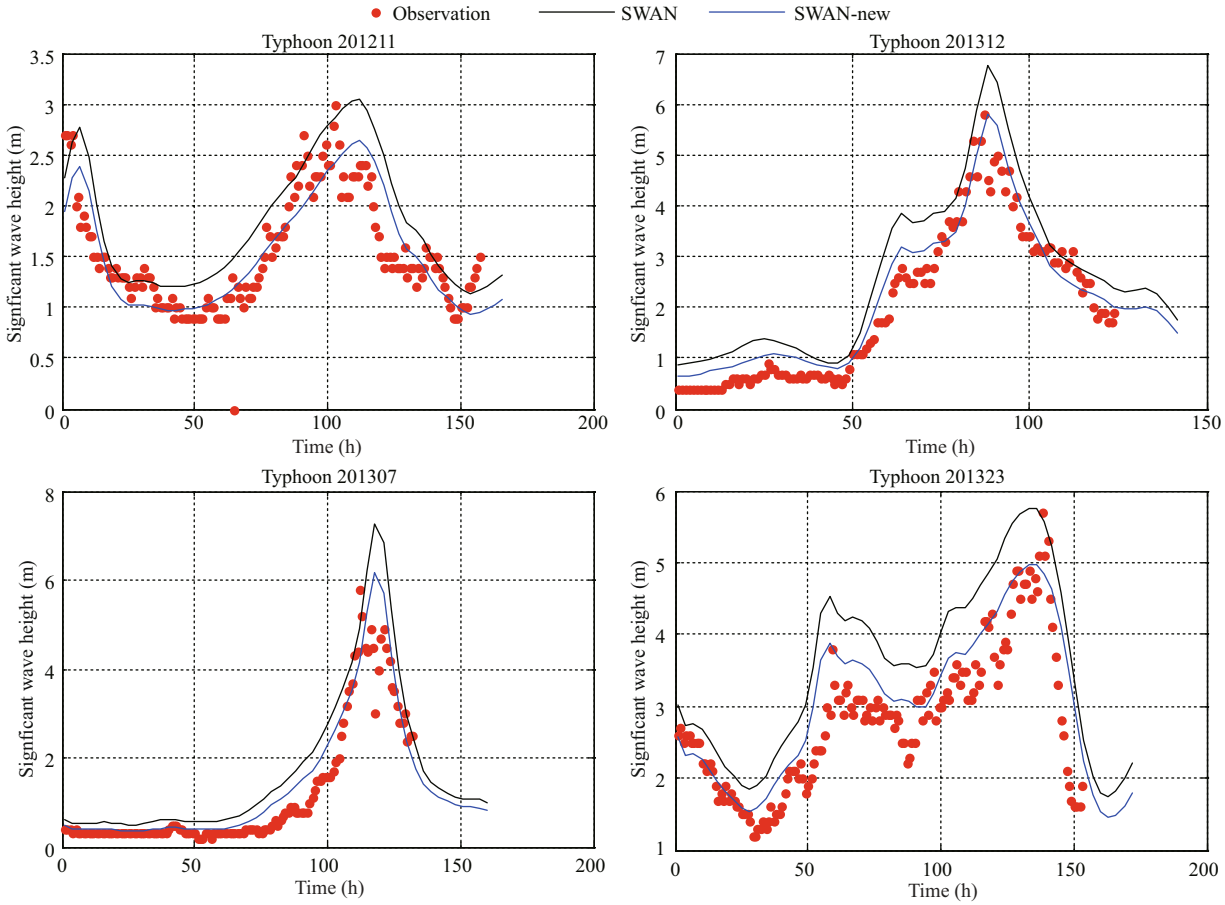

Fig.7 Comparisons of the significant wave height during four typhoons

$$\mathrm{ARE}=\frac{1}{N}\sum_{i=1}^{N}\left|\frac{X_{\mathrm{mod}}^{i}-X_{\mathrm{obs}}^{i}}{X_{\mathrm{obs}}^{i}}\right|\times 100\%. \qquad (25)$$

The SWAN model uses the drag coefficient of Wu (1980) while the SWAN-new model uses the drag coefficient obtained in the present paper. A significant wave height above 2 m is selected for model validation. The MAE of the significant wave height for the SWAN-new model is within 0.8 m while that for the SWAN model is as high as 1.36. ARE of the significant wave height for the SWAN-new model is within 15% while that for the SWAN model is as high as 31.1%. ARE and MAE of the SWAN-new model are thus lower than those of the SWAN model. The new drag coefficient thus performs better than the drag coefficient of the original SWAN model.

Table 4 ARE and MAE of significant wave heights for four typhoons

Typhoon		ARE (%)	MAE
201211	SWAN	18.0	0.48
	SWAN-new	13.8	0.42
201307	SWAN	23.4	1.36
	SWAN-new	14.1	0.78
201312	SWAN	17.2	0.67
	SWAN-new	10.7	0.44
201323	SWAN	31.1	1.05
	SWAN-new	14.6	0.54

5 CONCLUSION

Numerical modeling was established for wave forecasting in the Taiwan Strait and near Pingtan Island on the basis of the SWAN wave model. The SWAN wave model was used for the generation of waves by wind fields simulated using the WRF wind model. A triple triangular mesh was adopted, where the depth shoreline data included ETOPE1 data and nearshore measurements.

A reasonable drag coefficient was derived from the progress of nine typhoons using COARE 3.0. The progress of four typhoons was used to verify the effect of the drag coefficient on the typhoon wave model. Results indicate that simulation data agree well with observation data, and the new drag coefficient is better than that of the original SWAN model.

In summary, the present study clarified the effect of the drag coefficient on a typhoon wave model. The results of the study will benefit wave forecasting, wave disaster prediction, wave environment warning prediction, and emergency management.

6 DATA AVAILABILITY STATEMENT

The contents of this article are taken from the Research Data Archive. Further details can be viewed at the following websites.

1. NCEP/DOE Reanalysis 2 (R2): https://rda.ucar.edu/datasets/ds091.0/;

2. ETOPO1 Global Relief Model: https://www.ngdc.noaa.gov/mgg/global/.

7 ACKNOWLEDGEMENT

We thank Glenn Pennycook, MSc, from Liwen Bianji, Edanz Group China (www.liwenbianji.cn/ac), for editing the English text of a draft of this manuscript.

References

Alves J H G M, Banner M L. 2003. Performance of a saturation-based dissipation-rate source term in modeling the fetch-limited evolution of wind waves. *Journal of Physical Oceanography*, **33**(6): 1 274-1 298.

Booij N, Ris R C, Holthuijsen L H. 1999. A third-generation wave model for coastal regions: 1. Model description and validation. *Journal of Geophysical Research*: *Oceans*, **104**(C4): 7 649-7 666.

Bricheno L M, Soret A, Wolf J, Jorba O, Baldasano J M. 2013. Effect of high-resolution meteorological forcing on nearshore wave and current model performance. *Journal of Atmospheric and Oceanic Technology*, **30**(6): 1 021-1 037.

Cavaleri L, Malanotte Rizzoli P. 1981. Wind wave prediction in shallow water: theory and applications. *Journal of Geophysical Research*: *Oceans*, **86**(C11): 10 961-10 973.

Chalikov D, Babanin A V. 2012. Simulation of wave breaking in one-dimensional spectral environment. *Journal of Physical Oceanography*, **42**(11): 1 745-1 761.

Charnock H. 1955. Wind stress on a water surface. *Quarterly Journal of the Royal Meteorological Society*, **81**(350): 639-640.

Decharme B. 2007. Influence of runoff parameterization on continental hydrology: comparison between the Noah and the ISBA land surface models. *Journal of Geophysical Research*: *Atmospheres*, **112**(D19): D19108.

Dietrich J C, Zijlema M, Allier P E, Holthuijsen L H, Booij N, Meixner J D, Proft J K, Dawson C N, Bender C J, Naimaster A, Smith J M, Westerink J J. 2013. Limiters for spectral propagation velocities in SWAN. *Ocean Modelling*, **70**: 85-102.

Donelan M A, Haus B K, Reul N, Plant W J, Stiassnie M, Graber H C, Brown O B, Saltzman E S. 2004. On the limiting aerodynamic roughness of the ocean in very strong winds. *Geophysical Research Letters*, **31**(18): L18306.

Dudhia J. 1989. Numerical study of convection observed during the winter monsoon experiment using a mesoscale two-dimensional model. *Journal of the Atmospheric Sciences*, **46**(20): 3 077-3 107.

Eldeberky Y. 1996. Nonlinear Transformation of Wave Spectra in the Nearshore Zone. Ph. D. thesis, Delft University of Technology, Department of Civil Engineering, The Netherlands.

Fairall C W, Bradley E F, Hare J E, Grachev A A, Edson J B. 2003. Bulk parameterization of air-sea fluxes: updates and verification for the COARE algorithm. *Journal of Climate*, **16**(4): 571-591.

Fan Y L, Rogers W E. 2016. Drag coefficient comparisons between observed and model simulated directional wave spectra under hurricane conditions. *Ocean Modelling*, **102**: 1-13.

Hasselmann K. 1974. On the spectral dissipation of ocean waves due to white capping. *Boundary-Layer Meteorology*, **6**(1-2): 107-127.

Hasselmann S, Hasselmann K, Allender J H, Barnett T P. 1985. Computations and parameterizations of the nonlinear energy transfer in a gravity-wave spectrum. Part II: parameterizations of the nonlinear energy transfer for application in wave models. *Journal of Physical Oceanography*, **15**(11): 1 378-1 391.

Hong S Y, Noh Y, Dudhia J. 2006. A new vertical diffusion package with an explicit treatment of entrainment processes. *Monthly Weather Review*, **134**(9): 2 318-2 341.

Janssen P A E M. 1991. Quasi-linear theory of wind-wave generation applied to wave forecasting. *Journal of Physical Oceanography*, **21**(11): 1 631-1 642.

Kain J S, Fritsch J M. 1990. A one-dimensional entraining/detraining plume model and its application in convective parameterization. *Journal of the Atmospheric Sciences*, **47**(23): 2 784-2 802.

Kim Y, Jang S C, Lim T J. 2015. Hazard analysis of typhoon-related external events using extreme value theory. *Nuclear Engineering and Technology*, **47**(1): 59-65.

Komen G J, Hasselmann K, Hasselmann K. 1984. On the existence of a fully developed wind-sea spectrum. *Journal of Physical Oceanography*, **14**(8): 1 271-1 285.

Lee H S. 2015. Evaluation of WAVEWATCH III performance with wind input and dissipation source terms using wave buoy measurements for October 2006 along the east Korean coast in the East Sea. *Ocean Engineering*, **100**: 67-82.

Mlawer E J, Taubman S J, Brown P D, Iacono M J, Clough S A. 1997. Radiative transfer for inhomogeneous atmospheres: RRTM, a validated correlated-k model for the longwave. *Journal of Geophysical Research*: *Atmospheres*, **102**(D14): 16 663-16 682.

Moeini M H, Etemad-Shahidi A, Chegini V. 2010. Wave modeling and extreme value analysis off the northern

coast of the Persian Gulf. *Applied Ocean Research*, **32**(2): 209-218.

Oost W A, Komen G J, Jacobs C M J, Van Oort C. 2002. New evidence for a relation between wind stress and wave age from measurements during ASGAMAGE. *Boundary-Layer Meteorology*, **103**(3): 409-438.

Rascle N, Ardhuin F. 2013. A global wave parameter database for geophysical applications. Part 2: model validation with improved source term parameterization. *Ocean Modelling*, **70**: 174-188.

Ris R C, Holthuijsen L H, Booij N. 1999. A third-generation wave model for coastal regions: 2. verification. *Journal of Geophysical Research*: *Oceans*, **104**(C4): 7 667-7 681.

Roland A, Ardhuin F. 2014. On the developments of spectral wave models: numerics and parameterizations for the coastal ocean. *Ocean Dynamics*, **64**(6): 833-846.

Rusu E, Pilar P, Guedes Soares C. 2008. Evaluation of the wave conditions in Madeira archipelago with spectral models. *Ocean Engineering*, **35**(13): 1 357-13 71.

Siadatmousavi S M, Jose F, Stone G W. 2012. On the importance of high frequency tail in third generation wave models. *Coastal Engineering*, **60**: 248-260.

Skamarock W C, Klemp J B, Dudhia J, Gill D O, Barker D M, Duda M G, Huang X Y, Wang W, Powers J G. 2008. A Description of the Advanced Research WRF Version 3. NCAR/TN-475+STR NCAR/TN-475+STR. National Center for Atmospheric Research, Boulder, Colorado, USA. p.1-113.

Smith S D, Banke E G. 1975. Variation of the sea surface drag coefficient with wind speed. *Quarterly Journal of the Royal Meteorological Society*, **101**(429): 665-673.

Smith S D. 1988. Coefficients for sea surface wind stress, heat flux, and wind profiles as a function of wind speed and temperature. *Journal of Geophysical Research*: *Oceans*, **93**(C12): 15 467-15 472.

Takagaki N, Komori S, Suzuki N, Iwano K, Kurose R. 2016. Mechanism of drag coefficient saturation at strong wind speeds. *Geophysical Research Letters*, **43**(18): 9 829-9 835.

Taylor P K, Yelland M J. 2001. The dependence of sea surface roughness on the height and steepness of the waves. *Journal of Physical Oceanography*, **31**(2): 572-590.

Tolman H L. 1992. Effects of numerics on the physics in a third-generation wind-wave model. *Journal of Physical Oceanography*, **22**(10): 1 095-1 111.

Tsai Y S, Chang W T, Yu C M, Yang W C. 2018. General sea state and drag coefficient observed near shore in Taiwan Strait. *Procedia IUTAM*, **26**: 204-213.

Vickers D, Mahrt L, Andreas E L. 2013. Estimates of the 10-m neutral sea surface drag coefficient from aircraft eddy-covariance measurements. *Journal of Physical Oceanography*, **43**(2): 301-310.

WAMDI Group 1988. The WAM ModelA third gen-eration ocean wave prediction model. *Journal of Physical Oceanography*, **18**(12): 1 775-1 810.

Wang Y, Jiang X W. 2012. Improvement and application of a saturation based wave dissipation function in SWAN model. *Acta Oceanologica Sinica*, **31**(1): 24-32.

Wu J. 1982. Wind-stress coefficients over sea surface from breeze to hurricane. *Journal of Geophysical Research*: *Oceans*, **87**(C12): 9 704-9 706.

Yan L. 1987. An Improved Wind Input Source Term for Third Generation Ocean Wave Modelling. Scientific Report WR-No87-8, KNMI, De Bilt, The Netherlands.

Zhao D L, Li M X. 2018. Dependence of wind stress across an air–sea interface on wave states. *Journal of Oceanography*, 1-17. (in press)

Zijlema M, van der Westhuysen A J. 2005. On convergence behaviour and numerical accuracy in stationary SWAN simulations of nearshore wind wave spectra. *Coastal Engineering*, **52**(3): 237-256.

Zijlema M, van Vledder G P, Holthuijsen L H. 2012. Bottom friction and wind drag for wave models. *Coastal Engineering*, **65**: 19-26.